A Generalized Reflection-Free Domain-Truncation Method: Transparent Absorbing Boundary

Jian Peng and Constantine A. Balanis, *Fellow, IEEE*

***Abstract*— In this paper, a generalized technique is developed to truncate the computational domain without reflection. It transforms the unbounded-space Maxwell's equations to a set of auxiliary equations in a closed domain. A reflection-free amplitude-reduction scheme applied over the entire computational domain reduces the auxiliary field components outwardly and makes them equal to zero at the closed boundary. No additional absorbing region surrounding the domain of interest is needed with this technique because the relationship between the physical fields and their auxiliary counterparts is explicitly known and the former can be found from the latter within the computational domain.**

***Index Terms*—Absorbing media, FDTD methods.**

I. Introduction

In order to model and simulate an electromagnetic problem efficiently, it is necessary to minimize the computational domain that simulates an unbounded space. A variety of techniques, based either upon radiation mechanisms or upon absorption concepts, has been proposed [1]–[6]. They represent the fields with some prescribed conditions either at the exterior boundary of the computational domain or at the interface between the subject domain and the transition domain, as shown in Fig. 1. Ideally, a truncation technique should not create any reflections, at the boundaries where boundary conditions are enforced, to disturb the fields in the domain of the subject. In addition, it should be independent of the frequency and incident angle of the outwardly traveling waves. Moreover, it is preferred to reduce the computational domain as much as possible, especially by eliminating the transition domain surrounding the domain of interest (e.g., absorbing domain in absorption-based methods), to improve the computational efficiency.

The perfectly matched layer (PML) proposed by Berenger [6] is presently the state-of-art of truncation techniques. It is independent of frequency and incident angle and it is virtually reflection free. The PML is somewhat storage-intensive because it not only requires storing the fields in the additional absorbing domain, but it also splits the field components into two sets of subcomponents, which doubles its storage requirements. A variety of alternative approaches have since been proposed to avoid splitting of the fields [10], [11]; however, none of them eliminates the absorbing domain because they need the additional domain to attenuate the waves traveling out of the subject domain.

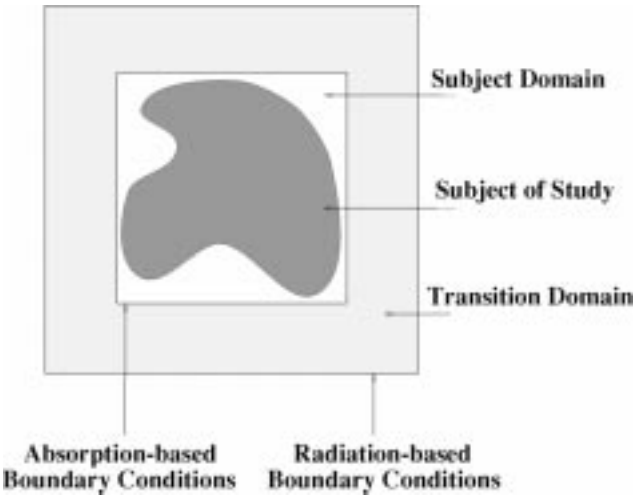

Fig. 1. A traditional computational domain.

The transparent absorbing boundary (TAB) [7]–[9] is a generalized analytical approach that can be directly applied to various finite methods such as finite difference and finite element in both time and frequency domains. Without introducing reflections, the magnitudes of the auxiliary field components *inside the subject domain* are forced to decrease and become exactly zero at the exterior boundary of *the same domain*. Consequently, the additional absorbing domain is no longer needed and the computational domain is reduced to the domain of interest (i.e., the subject domain in Fig. 1). In this paper, the basics of the TAB truncation method and the zero-reflection characteristics are detailed and its applications in the finite-difference time-domain (FDTD) method are also discussed.

II. Transparent Absorbing Boundary

The TAB method begins by introducing auxiliary fields that attenuate outwardly and become zero at the boundary of the subject domain. Constraints are imposed upon the auxiliary fields to ensure that no artificial reflections are introduced into the auxiliary system. Governing equations for the auxiliary system are derived from Maxwell's equations and are then solved for the auxiliary fields. After that the physical fields are found from the auxiliary ones through inverse transformation. In this section, the basic concepts and the transformation

Manuscript received March 28, 1996; revised April 14, 1998. This work was supported by NASA Langley Research Center Grant NAG1-1082 and the Advanced Helicopter Electromagnetics (AHE) Industrial Associates Program.

The authors are with the Department of Electrical Engineering, Telecommunications Research Center, Arizona State University, Tempe, AZ 85287 USA.

Publisher Item Identifier S 0018-926X(98)05778-0.

between the physical and auxiliary fields of the TAB are discussed.

A. Reflection-Free Transformation

Let $\mathbf{E}_o(t,r)$ and $\mathbf{H}_o(t,r)$ be the electric and magnetic fields of a physical problem in an unbounded space. They satisfy Maxwell's equations and the boundary conditions of a physical problem. Assume that $F(r)$ is a scalar amplitude modulation function. Then, a set of auxiliary fields $\mathbf{E}(t,r)$ and $\mathbf{H}(t,r)$ in the computational domain are defined as

$$\mathbf{E}(t,r) = F(r)\mathbf{E}_o(t,r) \tag{1a}$$

$$\mathbf{H}(t,r) = F(r)\mathbf{H}_o(t,r) \tag{1b}$$

for $r \leq r_o$ where r_o defines the closed truncation boundary. For example, in Fig. 1, r_o can be taken as the interface formed by the subject and transition domains.

It is well-known that there will be no reflection from an interface if the phase velocities and wave impedances on both sides of the interface are identical. Furthermore, no artificial reflections are introduced into a new field system if the boundary conditions, phase velocities, and wave impedances of the physical waves are maintained, i.e.,

$$[BC]_a = [BC]_o \tag{2a}$$

$$v_a = v_o \tag{2b}$$

$$\eta_a = \eta_o \tag{2c}$$

where the subscript o denotes the original system while subscript a indicates the auxiliary system whose field components decrease in a way prescribed by the outwardly decaying function $F(r)$. The field attenuation mechanism is superimposed upon the physical media and it creates no reflections regardless of frequency, incident angle, and physical material properties. In [6], it is indicated implicitly that the fields within the PML medium satisfy these conditions, which explains mathematically why the PML is a reflection-free loss mechanism.

If $F(r)$ in (1) is not equal to zero within the computational domain interior to the closed boundary, the auxiliary system has the same wave impedance as that of the physical system in the same region, i.e.,

$$\eta_a(r) = \frac{|\mathbf{E}(t,r)|}{|\mathbf{H}(t,r)|} = \frac{|\mathbf{E}_o(t,r)|}{|\mathbf{H}_o(t,r)|} = \eta_o(r) \tag{3}$$

where $\eta_o(r)$ represents the wave impedance of the physical problem, not necessarily the one in free-space. Furthermore, if the function F is continuous and real, the boundary conditions and phase terms of the auxiliary fields are the same as those of the physical problem. The phase velocity is a part of the phase term, hence, the two velocities are equal

$$v_a(r) = v_o(r). \tag{4}$$

Therefore, no artificial reflection is introduced by the transformation of (1) at any spatial point in the domain of the problem. In other words, the transformation seems *transparent*.

The above discussion is best illustrated by the plane wave example in Berenger's original paper. Within a PML medium, each of the field components is represented by (15) in [6], whose form is similar to (1), with

$$F(x,y) = \exp\left[-\frac{\sigma_x \cos\phi}{\epsilon_o c}x\right]\exp\left[-\frac{\sigma_y \sin\phi}{\epsilon_o c}y\right]. \tag{5}$$

In (5), c and ϕ are, respectively, the phase velocity and the incident angle in free-space, ϵ_o represents the free-space dielectric constant, and (σ_x, σ_y) are the anisotropic conductivities of the PML medium. Equation (5) indicates that the phase velocity of the attenuated wave in the PML is identical to that of the physical wave in the same free-space occupied by the PML. Meanwhile, (16) of [6] is identical to (3) in this paper; that is, the wave impedance of the attenuated field is not changed by the PML loss mechanism. Apparently, the PML and TAB are closely related.

While the attenuated fields in the PML region satisfy (1), the physical fields in the domain of interest can also be considered as auxiliary fields with F being unity. Therefore, the PML approach to solving for the fields in the entire computational domain is equivalent to finding the auxiliary fields of the TAB in the same domain. The difference between the PML and TAB is that their approaches are opposite. In the PML, (1) and (3) are derived from zero-reflection PML absorption, while the same equations lead to the reflection-free attenuation of fields in the TAB. In addition, the PML is associated with only one exponential F as given by (5). However, as will be demonstrated, the number of the amplitude modulation functions $F(r)$ for the TAB seems unlimited.

B. Field Attenuation

The role of the amplitude modulation function F is critical. It relates the auxiliary fields to the physical ones without distorting the phase and directional patterns of the physical fields. It also serves as an attenuation factor for the auxiliary fields. An example of the amplitude modulation function is shown in Fig. 2, which forces the magnitudes of the auxiliary fields to decay and eventually reduce them to zero at the exterior boundary of the computational domain. Due to its importance, it is necessary to set some criteria for the selection of the amplitude modulation function. The function should be defined over the computational domain only and it should:

1) be a single-valued, continuous, scalar real function;
2) decay as $\mathbf{r}$ increases outwardly and become zero at the exterior boundary;
3) be nonzero everywhere except along the exterior boundary of the subject domain;
4) have continuous first-order derivatives;
5) be independent of field information, as well as time.

The first two conditions are needed to establish the TAB conceptually, the next two to define the TAB mathematically, and the last one for the convenience of the inverse transformation from the auxiliary fields to the physical ones. The inverse transformation is an integral part of the TAB method and makes it possible to eliminate the additional absorbing domain. Apparently, the amplitude modulation function of the PML [as represented by (5)] satisfies all but the last condition. Hence, the PML creates no reflections; but it still needs the additional

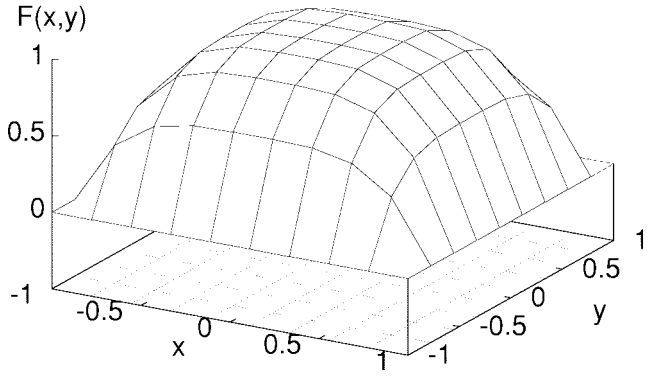

Fig. 2. A typical modulation function for the transparent absorbing boundary.

absorbing region, since the inverse transformation is generally not known in the PML layers and the physical fields cannot be recovered from the auxiliary fields inside the PML.

The conditions on the choice of F are quite easy to satisfy. In addition to the graphical illustration shown in Fig. 2

$$F(x,y,z) = \left[1 - \left(\frac{|x|}{L_x}\right)^m\right]^n \left[1 - \left(\frac{|y|}{L_y}\right)^p\right]^q \times \left[1 - \left(\frac{|z|}{L_z}\right)^u\right]^v \tag{6a}$$

and

$$F(x,y,z) = \cos^m\left[\frac{\pi}{2}\left(\frac{|x|}{L_x}\right)^n\right] \cos^p\left[\frac{\pi}{2}\left(\frac{|y|}{L_y}\right)^q\right] \times \cos^u\left[\frac{\pi}{2}\left(\frac{|z|}{L_z}\right)^v\right] \tag{6b}$$

are two analytical examples of F in Cartesian coordinates if m, n, p, q, u, and v are equal to or greater than unity. The parameters L_x, L_y, and L_z are the lengths of attenuation paths in the x, y, and z directions, respectively; they are often taken to be the half dimensions of a rectangular domain.

An amplitude modulation function satisfying the required conditions stated previously establishes a unique relationship between the physical and auxiliary fields so that the former can be found from the latter everywhere, except at the exterior truncation boundary where the function is equal to zero. Note that, *it is not necessary to find* $\mathbf{E}_o$ *and* $\mathbf{H}_o$ *exactly on the boundary*. The closed surface over which the equivalence principle is applied to find the far-zone $\mathbf{E}_o$ and $\mathbf{H}_o$ can be placed anywhere in the domain, as long as it is exterior to the subject of study and interior to the truncation boundary. Usually, this is chosen at one or two cells interior of the truncation boundary. With the help of this surface, the physical fields exterior to it can be obtained by integrating the currents on the surface, while those interior to the surface are found by inverting the auxiliary fields obtained with the finite methods. Therefore, a unique solution of the physical fields can be obtained in the entire unbounded space.

C. Governing Equations

While the physical fields $(\mathbf{E}_o, \mathbf{H}_o)$ are described by Maxwell's equations, governing equations for the auxiliary fields $(\mathbf{E}, \mathbf{H})$ in the closed domain are obtained by substituting $\mathbf{E}_o$ and $\mathbf{H}_o$ of (1) into Maxwell's equations. They are expressed in the form of

$$\frac{\partial \mathbf{E}}{\partial t} = \frac{1}{\epsilon}\left(\nabla \times \mathbf{H} - \frac{1}{F}\nabla F \times \mathbf{H}\right) - \frac{\sigma}{\epsilon}\mathbf{E} - \frac{F}{\epsilon} j_i \tag{7a}$$

$$\frac{\partial \mathbf{H}}{\partial t} = -\frac{1}{\mu}\left(\nabla \times \mathbf{E} - \frac{1}{F}\nabla F \times \mathbf{E}\right) - \frac{\sigma^*}{\mu}\mathbf{H} - \frac{F}{\mu} m_i \tag{7b}$$

$$\nabla \cdot \mathbf{E} = F\rho + \frac{1}{F}\nabla F \cdot \mathbf{E} \tag{7c}$$

$$\nabla \cdot \mathbf{H} = F\rho^* + \frac{1}{F}\nabla F \cdot \mathbf{H} \tag{7d}$$

with the boundary conditions of

$$\mathbf{E} = F(r_o)\mathbf{E}_o = \mathbf{0} \tag{7e}$$

$$\mathbf{H} = F(r_o)\mathbf{H}_o = \mathbf{0} \tag{7f}$$

where r_o denotes the truncating boundary, which is the exterior boundary for the domain of interest. It should be pointed out that the partial differential equations (7a)–(d) are valid in the entire closed domain *excluding the exterior truncation boundary* r_o. At $r = r_o$, the boundary conditions (7e) and (f), rather than the differential equations, are enforced. Obviously, the system has homogeneous boundary conditions because F decays and eventually becomes zero at the boundary $r = r_o$. The parameters σ, σ^*, j_i, m_i, ρ, and ρ^* retain their meanings of the physical problem [12]. Since F is a nonzero and single-valued scalar real function with continuous first-order derivatives within the closed domain, Maxwell's equations are uniquely transformed, along with the physical boundary conditions, into the auxiliary system. Hence, it is equivalent to solve the auxiliary system of (7) in the closed domain, rather than Maxwell's equations. For example, the attenuated fields in the PML region, as given by (15) in [6], can be obtained from (7) of this paper, with F being (5), instead of using the PML variations of Maxwell's equations.

The most important difference between the curl equations in (7) and those in Maxwell's equations is the introduction of the nondifferentiated terms $\frac{1}{F}\nabla F \times \mathbf{E}$ and $\frac{1}{F}\nabla F \times \mathbf{H}$. They represent losses or sources in a general hyperbolic system [13], [14]. With the outwardly decaying F, these two terms result in field attenuation for the outward wave and the introduction of the homogeneous boundary conditions (7e) and (f). The combination of the field attenuation and the transparent transformation leads to a reflection-free technique to truncate the computational domain of finite methods. Therefore, the method is referred to as the TAB, where *boundary* is used to follow standard nomenclature for the truncation of computational domains.

III. Applications in FDTD

In this section, the reflection characteristics of the TAB method will be detailed and some issues related to its application in the staggered Yee scheme will be discussed.

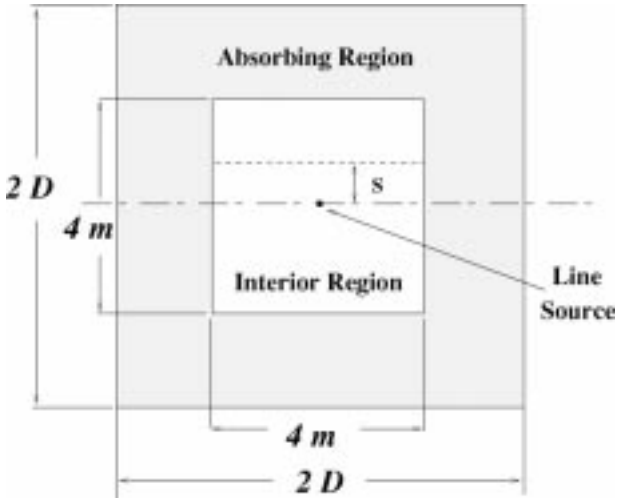

Fig. 3. Configuration of the testing computational domain.

A. Reflection Characteristics of the TAB

To demonstrate that, by using TAB, the introduction of an "absorbing" medium within the computational domain does not create reflections, the local reflection errors of a two-dimensional TM-polarized cylindrical wave were computed using the methodology suggested by Moore [15]. This procedure has been accepted and applied by many as a standard numerical technique to compute the reflections of absorbing boundary conditions in the time domain. Required by Moore's approach, the computational domain (2D $\times$ 2D) is subdivided into two regions, as shown in Fig. 3. The interior region is free space with dimensions of 4 m $\times$ 4 m. It is surrounded by an absorbing domain filled with absorbing materials. The fields inside the computational domain are excited by an E_z sinusoidal source placed at the center. The Yee algorithm is used to approximate (7a) and (b) and all computations were made with double precision.

Using the absorbing domain when testing TAB's reflections is not contradictory to the earlier claim that the the TAB does not need the additional absorbing domain. The errors under investigation are those reflected by the TAB medium rather than the total numerical errors. Those computed in the interior region usually include both the reflection errors of the TAB as well as the truncation errors of the finite-difference scheme. If the TAB is applied in the interior region only, (7a) and (b) instead of Maxwell's equations govern the field solution in the region. Consequently, Moore's method would not be able to cancel out the truncation errors with the solution of Maxwell's equations in a reference "open" domain. Therefore, it is necessary to use the extra absorbing domain in order to measure the reflections of the TAB. In practice, the total error instead of the reflection error is of concern; thus, the TAB applies the absorbing medium in the interior region only. The computational domain is then terminated at the boundary of the interior region.

The time duration is determined such that the measured reflections are created only by the TAB medium in the absorbing region and propagating into the interior region. This can be done by stopping field updating before the outgoing waves reach the exterior truncation boundary (the one exterior to the absorbing region in Fig. 3). The reason for doing so is as follows. In general, the reflections into the interior domain are the sum of two parts. One part stems from the numerical implementation such as the perfect electric conducting (PEC) termination used in the PML. The other part is due to the absorbing material itself. The former is not intrinsic to a particular analytical absorbing technique and it varies with numerical implementations. The latter is inherent to the absorbing mechanism itself and it is difficult to eliminate by changing implementation methods. Because of its staggered grids, the Yee scheme used along with the TAB presents an implementation error source that creates strong reflections. It has been shown that the problem is associated with staggered grids only [8], [9]. In the investigation of TAB's reflection characteristics, it is necessary to filter out the reflection errors that are not caused by the TAB media.

In the following tests, the field attenuation in the auxiliary system is prescribed by the amplitude modulation function

$$F(x,y)=\begin{cases}1 & \text{if } (x,y) \text{ in the interior domain}\\ f(x)g(y), & \text{otherwise}\end{cases} \tag{8a}$$

where

$$f(x)=1-\left(\frac{|x|-L}{D-L}\right)^4, \qquad \text{if } |x|>L \tag{8b}$$

$$g(y)=1-\left(\frac{|y|-L}{D-L}\right)^4, \qquad \text{if } |y|>L \tag{8c}$$

where $L=2$ m is the half dimension of the interior domain while D is that of the entire computational domain and may vary according to the thickness of the absorbing region used in the tests. Keep in mind that it is required by Moore's methodology (rather than the TAB truncation technique) to set the modulation function equal to unity $[F(x,y)=1]$ inside the interior domain. As a reference, the reflections of the PML were also computed, using the split formulation over the entire computational domain. The thickness of the PML region may vary between the tests, but the anisotropic conductivity of the PML is always quadratic in distribution, with $R(0)=10^{-12}$.

Using square cells of Δ, the finite-difference approximation to (7a) and (b) of the TM-polarized wave is given as follows:

$$H_x|_{i,j}^{n+\frac{1}{2}}=H_x|_{i,j}^{n-\frac{1}{2}}-\frac{\gamma}{\eta_o}\cdot\left[\left(1-\frac{\beta_j}{2}\right)E_z|_{i,j+\frac{1}{2}}^{n}-\left(1+\frac{\beta_j}{2}\right)E_z|_{i,j-\frac{1}{2}}^{n}\right] \tag{9a}$$

$$H_y|_{i,j}^{n+\frac{1}{2}}=H_y|_{i,j}^{n-\frac{1}{2}}+\frac{\gamma}{\eta_o}\cdot\left[\left(1-\frac{\alpha_i}{2}\right)E_z|_{i+\frac{1}{2},j}^{n}-\left(1+\frac{\alpha_i}{2}\right)E_z|_{i-\frac{1}{2},j}^{n}\right] \tag{9b}$$

$$E_z|_{i,j}^{n+1}=E_z|_{i,j}^{n}+\gamma\eta_o\left\{\left[\left(1-\frac{\alpha_i}{2}\right)H_y|_{i+\frac{1}{2},j}^{n+\frac{1}{2}}-\left(1+\frac{\alpha_i}{2}\right)H_y|_{i-\frac{1}{2},j}^{n+\frac{1}{2}}\right]-\left[\left(1-\frac{\beta_j}{2}\right)H_x|_{i,j+\frac{1}{2}}^{n+\frac{1}{2}}-\left(1+\frac{\beta_j}{2}\right)H_x|_{i,j-\frac{1}{2}}^{n+\frac{1}{2}}\right]\right\} \tag{9c}$$

where $\gamma=\frac{c\delta t}{\Delta}$ is the Courant number, $\eta_o=\frac{\mu_o}{\epsilon_o}$ is the wave impedance in free-space, and $(\alpha_i=\frac{\Delta f_i'}{f_i},\beta_j=\frac{\Delta g_j'}{g_j})$ are the

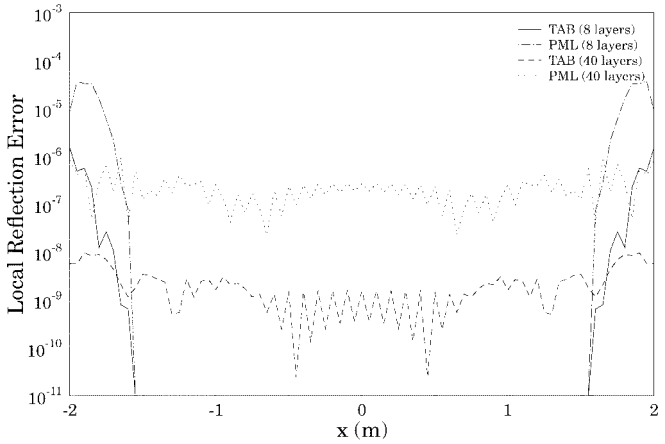

Fig. 4. Local reflection errors as a function of the thickness of the absorbing materials.

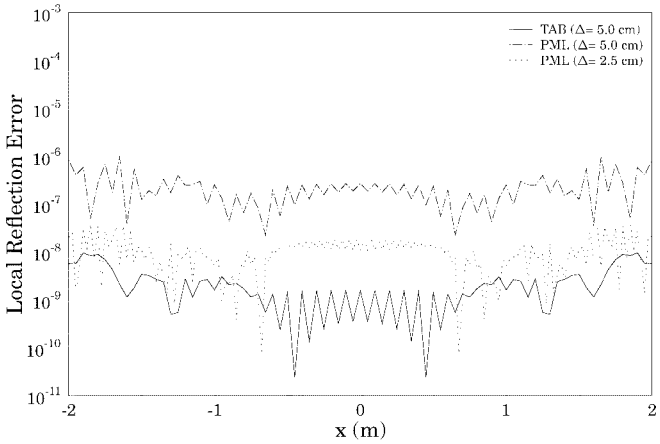

Fig. 5. Effect of reducing cell size on the local reflection error of the split PML.

coefficients associated with the introduction of the anisotropic TAB attenuation, respectively. The terms f' and g' represent the first-order spatial derivatives of f and g, respectively.

First, the effect of the attenuation length (i.e., the thickness of the absorbing domain) on the reflections are examined. The operating frequency is 300 MHz, the cell size Δ is 5 cm (i.e., $\frac{\lambda}{20}$), and the Courant number γ is 0.7. The local reflection errors are measured along dashed line shown in Fig. 3, with $s = 1$ m. Attenuation lengths of 0.4 m and 2.0 m (i.e., 8 and 40 cells) are used in the computations, respectively, and the time duration is 70 steps for the former while 100 steps are used for the latter. An eight-layer PML is commonly used in practice; using 40 layers makes the attenuation length equal to the distance from the source to the boundary of the subject domain, which enables the first reflected wavefront to get close to the center of the interior domain before the outgoing waves reach the exterior boundary. The results are shown in Fig. 4. With eight layers, the PML achieves a local reflection of 10^{-4} to 10^{-5} (or about -90 dB) while that of the TAB is about 20 dB lower ($\simeq -110$ dB). Using 40 layers makes the attenuation functions (exponential for the PML and polynomial for the TAB) flatter along the attenuation path, which results in better finite-difference approximations. The smoother amplitude modulations yield about 40-dB improvements for both the PML and TAB.

The difference between the PML and TAB results is attributed to the split formulation, which is only an approximate equivalence to Maxwell's equations [17]. To reduce the effect of this approximated equivalence, the cell size for the split formulation is reduced by half. Since the split formulas are second-order approximations to the Maxwell's equations, the discrepancy between Maxwell's equations and its split counterparts is reduced by a factor of four. Meanwhile, the truncation errors of the second-order Yee finite difference that approximates the split formulas are also reduced by a factor of four. Totally, the numerical errors are reduced by a factor of 16. Fig. 5 shows the results for the case of 2.0 m (40 cells) absorbing region. Using the smaller cells reduces the local reflection error of the PML and the reduction shows the behavior of second-order approximations. Thus, the extra errors in the PML computations are introduced most likely by the split equations instead by the loss mechanism of the PML.

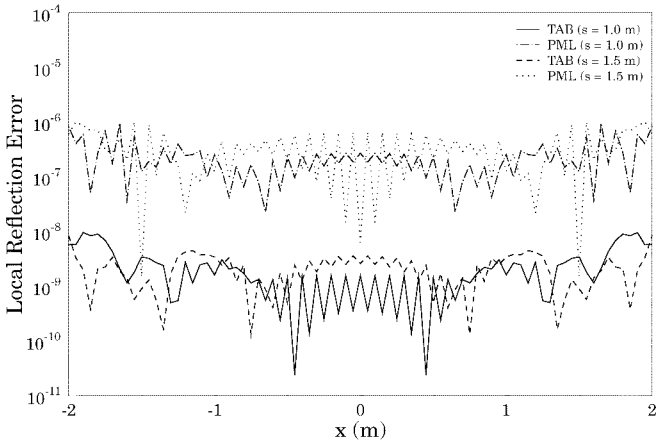

Fig. 6. Local reflection errors that are independent of incident angles.

Next, the dependence of the TAB on the incident angle is investigated by collecting data along the lines $s = 1$ m and $s = 1.5$ m, respectively. At a given position x, the reflections on the two lines are from different reflection angles. The operating frequency is 300 MHz, the cell size Δ is 5 cm, and the Courant number γ is 0.7. The attenuation length is 2.0 m (i.e., 40 cells), while the time duration is 100 steps. Like the PML, the TAB has similar local reflection errors along the two different lines, as shown in Fig. 6, which indicates that the the loss mechanism is independent of the incident angle.

Finally, the TAB's independence of frequency is verified in Fig. 7. The attenuation length, cell size Δ, Courant number γ, and time duration are the same as those of Fig. 6. The operating frequencies are 150 and 300 MHz, respectively. Reflection errors were measured along the line $s = 1$ m. As is expected, the computed local reflection errors are independent of the frequency for both the PML and TAB. Thus far, it has been demonstrated numerically that the TAB is a reflection-free loss mechanism like the established PML.

B. Application of the TAB to FDTD

The development of the TAB is to provide an alternative method to truncate a computational domain without intro-

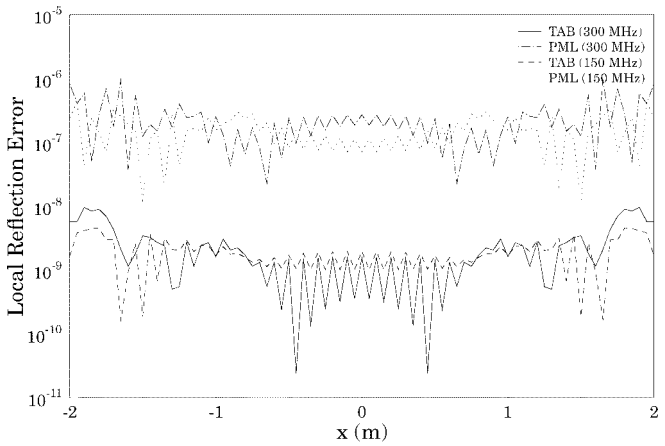

Fig. 7. Local reflection errors that are independent of frequencies.

ducing artificial reflections. It has been shown that the TAB successfully truncates the computational domain of the collocated Lax–Wendroff finite-difference scheme [8], [9]. It also was shown in the previous section that the TAB itself does not create reflections. However, when used with the Yee algorithm that is not a collocated scheme for $\mathbf{E}$ and $\mathbf{H}$, the TAB presents some challenging issues.

The Artificial Metal Wall: In the Yee scheme, the electric and magnetic fields are *staggered*, i.e., they are located a half-cell apart. An one-dimensional (1-D) illustration of the staggered grids is illustrated in Fig. 8. Applying Yee's algorithm to the H field of the 1-D problem results in the finite-difference equation

$$H|_{i+\frac{1}{2}}^{n+\frac{1}{2}} = H|_{i+\frac{1}{2}}^{n-\frac{1}{2}} - \frac{\gamma}{\eta_o}\left[\left(1-\frac{\alpha_{i+\frac{1}{2}}}{2}\right)E|_{i+1}^{n} - \left(1+\frac{\alpha_{i+\frac{1}{2}}}{2}\right)E|_{i}^{n}\right]. \quad (10)$$

When $i = N-1$, which represents the H-field point next to the truncation boundary, (10) reduces to

$$H|_{N-\frac{1}{2}}^{n+\frac{1}{2}} = H|_{N-\frac{1}{2}}^{n-\frac{1}{2}} - \frac{\gamma}{\eta_o}\left[\left(1-\frac{\alpha_{N-\frac{1}{2}}}{2}\right)E|_{N}^{n} - \left(1+\frac{\alpha_{N-\frac{1}{2}}}{2}\right)E|_{N-1}^{n}\right] \quad (11)$$

where $E|_N^n$ is on the homogeneous truncation boundary and it is equal to zero because $f_N = 0$. Although the next-to-last electric field point $E|_{N-1}^n$ is not on the boundary, the coefficient associated with it is

$$1+\frac{\alpha_{N-\frac{1}{2}}}{2} = 1+\frac{\Delta f'_{N-\frac{1}{2}}}{2f_{N-\frac{1}{2}}} = \frac{f_{N-\frac{1}{2}}+\frac{\Delta}{2}f'_{N-\frac{1}{2}}}{f_{N-\frac{1}{2}}} \approx \frac{f_N}{f_{N-\frac{1}{2}}} = 0. \quad (12)$$

Consequently, the spatial difference in (11) is nearly zero, which reduces the equation to

$$H|_{N-\frac{1}{2}}^{n+\frac{1}{2}} \simeq H|_{N-\frac{1}{2}}^{n-\frac{1}{2}}. \quad (13)$$

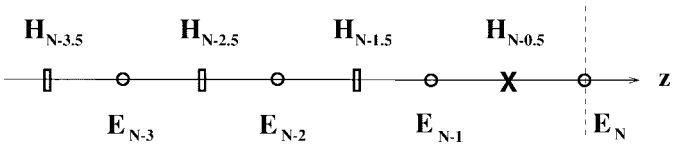

Fig. 8. One-dimensional illustration of a staggered grid, such as Yee's.

That is, the value of $H|_{N-\frac{1}{2}}^{n+\frac{1}{2}}$ depends mainly on its previous value $H|_{N-\frac{1}{2}}^{n-\frac{1}{2}}$. If the initial value is zero, $H|_{N-\frac{1}{2}}$ will be close to zero for all the time steps. Since the E component at that spatial position is not subject to the near-zero condition, the fact that $H_{N-\frac{1}{2}}$ is always close to zero is equivalent to a magnetic conducting wall at the position. Similarly, an electric conducting wall can be formed if the truncation boundary falls on the H instead of E field points. These artificial electric/magnetic conducting walls reflect fields strongly, which is not desirable for a domain truncation technique.

It should be pointed out that the artificial electric/magnetic conducting walls are only associated with *staggered* finite-difference schemes (such as the Yee scheme). In *collocated* schemes, like the Lax–Wendroff, both E and H are subject to identical near-zero conditions; both components are very small near the truncation boundary due to the "absorption" of the TAB. Therefore, there exist no such artificial walls in collocated schemes, as is demonstrated in [9].

One way to circumvent the problem is to modify the finite-difference scheme near the truncation boundary such that the fields next to the truncation boundary will not be near zero all the time. The Lax–Friedrichs scheme [19] is used to replace the Yee scheme at the grid points half-cell interior to the truncation boundary. The scheme uses spatially averaged values in the time differencing. Thus, the finite-difference equation at the last H point becomes

$$\begin{aligned} H|_{N-\frac{1}{2}}^{n+\frac{1}{2}} &= \frac{1}{2}\left(H|_{N-1}^{n-\frac{1}{2}} + H|_{N}^{n-\frac{1}{2}}\right) \\ &\quad - \frac{\gamma}{\eta_o}\left[\left(1-\frac{\alpha_{N-\frac{1}{2}}}{2}\right)E|_{N}^{n} - \left(1+\frac{\alpha_{N-\frac{1}{2}}}{2}\right)E|_{N-1}^{n}\right] \\ &= \frac{1}{2}H|_{N-1}^{n-\frac{1}{2}} + \frac{\gamma}{\eta_o}\left(1+\frac{\alpha_{N-\frac{1}{2}}}{2}\right)E|_{N-1}^{n} \simeq \frac{1}{2}H|_{N-1}^{n-\frac{1}{2}} \end{aligned} \quad (14)$$

instead of (11) and (13). In (14), H_{N-1} is the field at the grid that is a *one*-cell, instead of a *half*-cell, interior to the truncation boundary. With this local modification, the field variation near the half-cell point will be channeled into it through the averaging process and the $H_{N-\frac{1}{2}}$ will not be close to zero all the time. Therefore, the effects of the magnetic conducting wall are reduced. The challenge of this local modification is to find the appropriate value for $H|_{N-1}^{n-\frac{1}{2}}$ in (14) since it is located between two H grid points. Interpolations using the existing H grids were tested.

To test the effect of the local modifications near the truncation boundary, a 1-D problem is examined numerically, using the following configuration. The computational domain is $2L = 4$ m in length and it is discretized with $\Delta = 0.025\lambda$ cells. A plane wave source is located in the middle of the

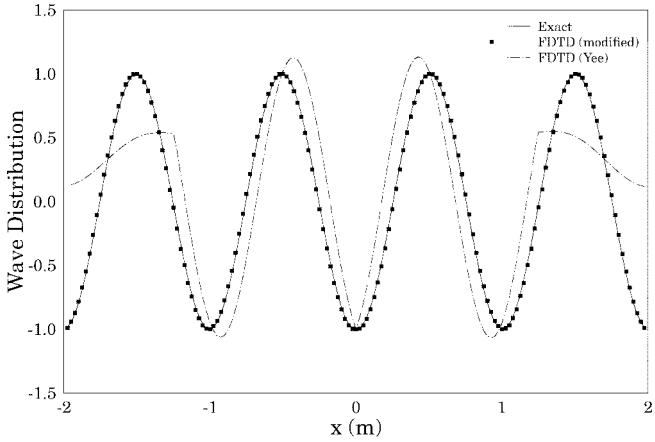

Fig. 9. One-dimensional field distribution E_o of a plane wave traveling outwardly in both directions obtained using Yee's staggered scheme.

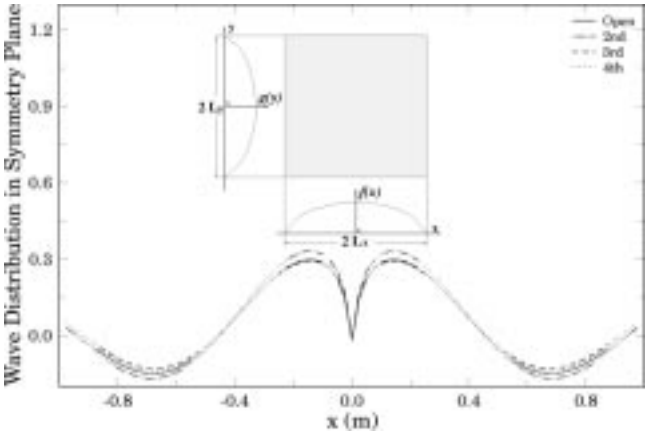

Fig. 10. Field distribution along the symmetry plane of a 2-D problem obtained with an entire domain F.

domain and the wave propagates in both directions. The following amplitude modulation function is used to terminate the domain:

$$f(x) = 1 - \left(\frac{|x|}{L}\right)^4, \qquad \text{if } |x| \le L. \tag{15}$$

The Courant number is chosen as 1; the time duration is 400 steps, which is sufficiently long for the artificial reflected waves to bounce back and forth a few times between the boundary points to show the effect of reflection errors on the results (it takes 80 steps for the plane wave to travel from the source to the boundaries and vice versa). The local modification of (14) replaces the Yee scheme of (11) at the last H point. The second-order interpolation of

$$H|_{N-1}^{n-\frac{1}{2}} = \frac{1}{2}\left(H|_{N-0.5}^{n-\frac{1}{2}} + H|_{N-1.5}^{n-\frac{1}{2}}\right) \tag{16}$$

is used to find the H_{N-1} that is collocated with E_{N-1}. The computed auxiliary E field is converted back to E_o, and compared with the exact solution. The numerical results are shown in Fig. 9. The results represented by the dash-dot line were obtained using Yee's scheme without any local modification near the exterior truncation boundary. They are not in good agreement with the exact solution. The square dots represent the results computed with the local modified scheme, as represented by (14) and (16); they agree quite well with the exact solution.

However, it was found that the effectiveness of the interpolation given in (16) depends on the choice of the Courant number $\gamma = \frac{c\delta t}{\Delta}$; $\gamma = 1$ happens to be the optimal value for the second-order interpolation. The third-order interpolation

$$H|_{N-1}^{n-\frac{1}{2}} = H|_{N-0.5}^{n-\frac{1}{2}} + \frac{1}{3}H|_{N-1.5}^{n-\frac{1}{2}} \tag{17}$$

and the fourth-order one

$$H|_{N-1}^{n-\frac{1}{2}} = \frac{3}{4}H|_{N-0.5}^{n-\frac{1}{2}} + \frac{1}{2}H|_{N-1.5}^{n-\frac{1}{2}} - \frac{1}{20}H|_{N-2.5}^{n-\frac{1}{2}} \tag{18}$$

may provide alternatives to different γ values. Using the Lax–Friedrichs scheme near the boundary is one of many possible techniques to reduce the effects of the artificial electric/magnetic conducting walls and others may be even more desirable.

The Effect of the Interpolation Schemes: As mentioned in the previous section, the effectiveness of an interpolation scheme, used to find the fields between regular grid points depends on the the value of γ. In a 2-D problem, γ has to be smaller than $\frac{1}{\sqrt{2}}$ because of the stability condition. In this section, the effects of the interpolation schemes on the reduction of the reflections from the artificial magnetic conducting walls are examined.

The 2-D Yee scheme for a TM polarized case is given in (9). The amplitude modulation function

$$F(x,y) = f(x)g(y) = \left[1 - \left(\frac{|x|}{L_x}\right)^4\right]\left[1 - \left(\frac{|y|}{L_y}\right)^4\right] \tag{19}$$

is defined over the entire $2L_x \times 2L_y$ square domain shown as the insert in Fig. 10 with $L_x = L_y = 1$ m. An E_z sinusoidal source is placed at the center of the domain operating at 300 MHz. The cell size is 0.025 λ, the Courant number is chosen to be 0.7, and the time duration is 200 steps that is sufficiently long to show the effects of the reflection due to the artificial magnetic conducting wall (it takes about 60 steps for a wave to travel from the center to the boundary or vice versa). The results are inversely transformed and then compared with the "open" space computations that were performed for the same time duration in a 8 m $\times$ 8 m domain discretized using the same cell size. All the calculations were performed with single precision.

Fig. 10 shows the distribution of the E_z component along the symmetry plane with different interpolation schemes. The second-order interpolation scheme of (16) does not perform as well as it did in the 1-D case, because $\gamma = 0.7$ is not its optimum value. The higher order interpolations of (17) and (18) helped to reduce the reflection and improved the numerical results noticeably; but efforts such as finding the optimum γ for the third- or fourth-order interpolations are needed to reduce the errors even further.

The global root mean square (rms) errors

$$\text{rms} = \frac{1}{N_x N_y}\sqrt{\sum_{i=1,j=1}^{N_x,N_y} |E_z|_{i,j}(\text{closed}) - E_z|_{i,j}(\text{open})|^2} \tag{20}$$

TABLE I
GLOBAL ERRORS ASSOCIATED WITH INTERPOLATION SCHEMES

	2nd	3rd	4th
RSM	2.13×10^{-4}	1.23×10^{-4}	8.9×10^{-5}
$FRSM$	0.1426	0.0821	0.0594

as well as global fractional rms (frms) errors

$$\text{frms} = \sqrt{\frac{\sum_{i=1,j=1}^{N_x,N_y} |E_z|_{i,j}(\text{closed}) - E_z|_{i,j}(\text{open})|^2}{\sum_{i=1,j=1}^{N_x,N_y} |E_z|_{i,j}(\text{open})|^2}} \quad (21)$$

for the results of Fig. 10 were also calculated. It is noted that because the modulation function of (19) is used over the entire computational domain, (20) and (21) calculate the total numerical errors instead of the reflection errors. Table I lists the computed errors and it shows that with the Lax–Friedrichs scheme and interpolations for the local modification near the truncation boundary, it is possible to achieve numerical accuracy comparable to the Mur's absorbing boundary conditions [2]. Other approaches should be explored in order to exploit the potential of the TAB with Yee's staggered scheme. This is presented as a challenge and further research to the computational electromagnetics community.

IV. CONCLUSION

An analytical approach, the TAB, has been presented. The domain truncation method focuses on the consequence of field attenuation rather than the causes of "absorption." The conditions on the transparent transformation are simple and a large family of amplitude modulation functions can be used for domain truncation without creating reflections. In addition, the method can be directly applied to time- and frequency-domain finite methods without modifications to its partial differential equations. Hence, it is a general approach to computational domain truncation.

With the TAB method, a physical problem in an unbounded space can be solved in a closed domain with the aid of the auxiliary fields. Like the popular PML method, the TAB is reflection-free, independent of frequency, and unconstrained by the incident angle. The uniqueness of the TAB is that it does not need the additional absorbing domain. In addition, it is suitable to truncate comformally an arbitrary convex domain by defining the amplitude modulation function F according to the geometry of the domain.

The TAB itself does not create reflections, as demonstrated by the examples in this paper and [9]. However, using the TAB along with the popular Yee staggered algorithm, an artificial electric/magnetic conducting wall is formed near the exterior boundary. Such a problem is associated only with staggered schemes and is presented as a future challenge. The Lax–Friedrichs scheme was tested as a local modification near the truncation boundary to prevent the formation of these artificial walls. Other approaches should be explored in order to effectively use the TAB to truncate the staggered Yee grids. Hopefully, the strengths and challenging issues of the TAB will stimulate new ideas and further research to improve the computational efficiency and accuracy of finite methods.

REFERENCES

[1] B. Engquist and A. Majda, "Absorbing boundary conditions for the numerical simulation of waves," *Math. Comput.*, vol. 31, pp. 629–651, 1977.

[2] G. Mur, "Absorbing boundary conditions for the finite-difference approximation of the time-domain electromagnetic field equations," *IEEE Trans. Electromagn. Compat.*, vol. EMC-23, pp. 377–382, Nov. 1981.

[3] Z. P. Liao, H. L. Wong, B. P. Yang, and Y. F. Yuan, "A transmitting boundary for transient wave analyses," *Scientia Sinica*, vol. XXVII, ser. A, pp. 1063–1076, 1984.

[4] R. L. Higdon, "Numerical absorbing boundary conditions for the wave equation," *Math. Comput.*, vol. 49, pp. 65–90, 1987.

[5] K. K. Mei and J. Fang, "Superabsorption—A method to improve absorbing boundary conditions," *IEEE Trans. Antennas Propagat.*, vol. 40, pp. 1001–1010, Sept. 1992.

[6] J. P. Berenger, "A perfectly matched layer for the absorption of electromagnetic waves," *J. Computat. Phys.*, vol. 114, no. 2, pp. 185–200, Oct. 1994.

[7] J. Peng and C. A. Balanis, "A new reflection-free truncation in finite methods: Transparent absorbing technique (TAT)," in *IEEE Antennas Propagat. Soc. Int. Symp.*, Baltimore, MD, July 1996, vol. 1, pp. 88–91.

[8] ——, "Transparent absorbing boundary (TAB): Truncation of computational domain without reflections," in *Appl. Comput. Electromagn. Soc. (ACES) 13th Annu. Progress Rev.*, Monterey, CA, Mar. 1997, vol. 1, p. 90.

[9] ——, "Transparent absorbing boundary (TAB) for the truncation of the computational domain," *IEEE Microwave Guided Wave Lett.*, vol. 7, pp. 347–349, Nov. 1997.

[10] Z. S. Sacks, D. M. Kingsland, R. Lee, and J. Lee, "A perfectly matched anisotropic absorber for use as an absorbing boundary condition," *IEEE Trans. Antennas Propagat.*, vol. 43, pp. 1460–1463, Dec. 1995.

[11] W. C. Cho and W. H. Weedon, "A 3-D perfectly matched medium from modified Maxwell's equations with stretched coordinates," *Microwave Opt. Technol. Lett.*, vol. 7, pp. 599–604, Sept. 1994.

[12] C. A. Balanis, *Advanced Engineering Electromagnetics*. New York: Wiley, 1989.

[13] P. R. Garabedian, *Partial Differential Equations*. New York: Wiley, 1964.

[14] F. Mainardi and D. Cocci, "Energy propagation in linear hyperbolic systems in the presence of dissipation," in *Nonlinear Hyperbolic Problems: Theoretical, Appl. Computat. Aspects, Proc. 4th Int. Conf. Hyperbolic Problems*, Taormina, Italy, Apr. 1992, pp. 409–415.

[15] T. G. Moore, J. G. Blaschel, A. Taflove, and G. A. Kriegsmann, "Theory and application of radiation boundary operators," *IEEE Trans. Antennas Propagat.*, vol. 36, pp. 1797–1812, Dec. 1988.

[16] K. S. Yee, "Numerical solution of initial boundary value problems involving Maxwell's equations in isotropic media," *IEEE Trans. Antennas Propagat.*, vol. AP-14, pp. 302–307, Mar. 1966.

[17] P. L. Roe, "Discontinuous solutions to hyperbolic systems under operator splitting," *Numer. Methods Partial Differential Eqs.*, vol. 7, no. 3, pp. 277–297, 1991.

[18] P. D. Lax and B. Wendroff, "Systems of conservation laws," *Commun. Pure Appl. Math.*, vol. 13, pp. 217–237, 1960.

[19] R. D. Richtmyer and K. W. Morton, *Difference Methods for Initial-Value Problems*, 2nd ed. New York: Wiley, 1967.

Jian Peng was born in Jiangsu, China, in 1959. He received the B.S.E.E. degree from the University of Electrical Science and Technology of China (formerly Chengdu Institute of Radio Engineering), Chengdu, China, in 1982, and the M.S. degree in electrical engineering from Arizona State University, Tempe, AZ, in 1992. He is currently working toward the Ph.D. degree at the same university.

Currently, he is with the Wireless Infrastructure System Division of Motorola, Phoenix, AZ. His research interests include computational electromagnetics, packaging simulation, antenna analysis, electromagnetic compatibility, and electromagnetic interference.

Constantine A. Balanis (S'62–M'65–SM'74–F'86), for photograph and biography, see p. 259 of the February 1998 issue of this TRANSACTIONS.